

# Elastic Interaction between a Vortex Dipole and an Axisymmetrical Vortex in Two-Dimensional Flows

Victoria Christine Zoeller<sup>1</sup> and Alvaro Viudez<sup>2</sup>

<sup>1</sup>Institute of Marine Sciences

<sup>2</sup>Institute of Marine Sciences, Spain

November 23, 2022

## Abstract

We investigate numerically the elastic interaction between a dipole and an axisymmetrical vortex in inviscid isochoric two-dimensional flows satisfying Euler's vorticity conservation equation. This work contributes to previous studies addressing inelastic vortex interactions. The dipole is a straight moving Lamb-Chaplygin (L-C) vortex, where the absolute value of either the positive or the negative amount of vorticity equals the amount of vorticity of the target vortex. The results show that, when the straight moving L-C dipole approaches the axisymmetrical vortex, the potential flows of both vortices interact, the dipole's trajectory acquires curvature and the dipole's vorticity poles separate. Once the L-C dipole moves away from the target vortex, the poles close and the dipole continues with a straight trajectory but along a direction different from the initial one. Though there is very small vorticity exchange between the dipole's poles and a small vorticity leakage to the background field, the vortices preserve, to a large extent, their amount of vorticity and the resulting interaction may be practically qualified as an elastic interaction. This process is sensitive to the initial conditions and, depending on the initial position of the dipole as well as on small changes in the vorticity distribution of the axisymmetrical vortex, inelastic interactions may instead occur. Since the initial vorticity distributions are based on the eigenfunctions of the two-dimensional Laplacian operator in circular geometry these results are directly applicable to three-dimensional baroclinic geophysical flows under the quasi-geostrophic approximation.

# Elastic Interaction between a Vortex Dipole and an Axisymmetrical Vortex in Two-Dimensional Flows

V. Zoeller<sup>1</sup>, A. Viúdez<sup>1</sup>

<sup>1</sup>Department of Physical Oceanography and Technology, Institute of Marine Sciences, CSIC, Barcelona 08003, Spain

## Key Points:

- Numerical description of an elastic interaction between a Lamb-Chaplygin dipole and an axisymmetrical vortex in two-dimensional flows
- Numerical simulations of inelastic interactions with vortex partner exchange, merging and straining out processes
- Results are applicable to three-dimensional baroclinic geophysical flows under the quasi-geostrophic approximation

---

Corresponding author: Victoria Zoeller, [zoeller@icm.csic.es](mailto:zoeller@icm.csic.es)

**Abstract**

We investigate numerically the elastic interaction between a dipole and an axisymmetrical vortex in inviscid isochoric two-dimensional flows satisfying Euler's vorticity conservation equation. This work contributes to previous studies addressing inelastic vortex interactions. The dipole is a straight moving Lamb-Chaplygin (L-C) vortex, where the absolute value of either the positive or the negative amount of vorticity equals the amount of vorticity of the target vortex. The results show that, when the straight moving L-C dipole approaches the axisymmetrical vortex, the potential flows of both vortices interact, the dipole's trajectory acquires curvature and the dipole's vorticity poles separate. Once the L-C dipole moves away from the target vortex, the poles close and the dipole continues with a straight trajectory but along a direction different from the initial one. Though there is very small vorticity exchange between the dipole's poles and a small vorticity leakage to the background field, the vortices preserve, to a large extent, their amount of vorticity and the resulting interaction may be practically qualified as an elastic interaction. This process is sensitive to the initial conditions and, depending on the initial position of the dipole as well as on small changes in the vorticity distribution of the axisymmetrical vortex, inelastic interactions may instead occur. Since the initial vorticity distributions are based on the eigenfunctions of the two-dimensional Laplacian operator in circular geometry these results are directly applicable to three-dimensional baroclinic geophysical flows under the quasi-geostrophic approximation.

**Plain Language Summary**

Ocean swirls, also known as eddies or vortices are ubiquitous in all oceans. Often they drift as two vortices together, rotating in opposite direction, known as eddy-pairs. The eddy-pair can encounter with different structures as well as with other ocean vortices. Here we prove that elastic interaction between two vortices are possible, meaning that the interaction does not change the vorticity properties of the vortices. We also describe numerically inelastic interactions, where the dipole (vortex-pair) separates or loses part of its vorticity. We use a two-dimensional model as many geophysical ocean processes occur on an approximately horizontal scale, though we show that the results given are also applicable to three-dimensional baroclinic flows.

**1 Introduction**

Mesoscale and submesoscale vortical structures are ubiquitous in the oceans and atmosphere. In particular, cyclonic and anticyclonic vortices are found in different configurations, including monopoles, dipoles, and tripoles. Specifically, vortex dipoles, also known as vortex pairs or couples, double vortices, modons, or mushroom-like vortices have been observed all over the oceans. Some examples include vortex pairs of the southern coast of Madagascar (de Ruijter et al., 2004; Ridderinkhof et al., 2013), eastern of Australia (Li et al., 2020), the Norwegian coast (Johannessen et al., 1989), the Mexican coast (Santiago-García et al., 2019), California coast (Sheres & Kenyon, 1989), in the Alaska current (Ahlén et al., 1987), in the South China Sea (Huang et al., 2017) and along the Canary Islands (Barton et al., 2004). These dipoles are generated by different causes, including the instability of baroclinic currents (Carton, 2001), localized forcing in a viscous stratified fluid (Voropayev & Afanasyev, 1994), or coastal interaction (de Ruijter et al., 2004).

The dipole structure and its stability has been subject of many experimental, laboratory, and numerical studies (Couder & Basdevant, 1986; Flór & Van Heijst, 1994; Rasmussen et al., 1996; Voropayev & Afanasyev, 1994). The dipole possesses a propagation speed, and may be considered as the simplest self-induced translating vortex structure (Afanasyev, 2003; Carton, 2001). For this reason it can interact with,

for example, a sloping boundary (Kloosterziel et al., 1993), a submarine mountain (Zavala Sansón & Gonzalez, 2021), a coastline (de Ruijter et al., 2004), inertia–gravity waves (Claret & Viúdez, 2010; Huang et al., 2017), other dipoles (Afanasyev, 2003; Dubosq & Viúdez, 2007; McWilliams & Zabusky, 1982; Velasco Fuentes & Heijst, van, 1995; Voropayev & Afanasyev, 1992) or other multipolar vortices (Besse et al., 2014; Viúdez, 2021; Voropayev & Afanasyev, 1992). Most of these interactions seem to be inelastic, in the sense that the vorticity dipole suffers irreversible changes during the interaction, for example during vortex merging or partial or complete straining out processes (Dritschel, 1995; Dritschel & Waugh, 1992; Dubosq & Viúdez, 2007; McWilliams & Zabusky, 1982; Voropayev & Afanasyev, 1992). However, in many instances ocean vortices do not interact strongly with one another for long time periods (Carton, 2001). Consequently, elastic interactions, where vorticity exchange does not occur, are also possible between ocean vortices. In this study we investigate numerically, as a particular kind of elastic dipole–vortex interaction, the interaction between a translating dipole and an axisymmetrical vortex.

In view of the complexity of baroclinic three-dimensional (3D) vortices, it is more practical to investigate first the barotropic two-dimensional (2D) case, assuming an adiabatic, inviscid, and incompressible fluid, satisfying the Euler equation of motion, which in this case reduces to the material conservation of vertical vorticity  $\zeta(\mathbf{x}, t) \equiv \mathbf{k} \cdot \nabla \times \mathbf{u}(\mathbf{x}, t)$ , where  $\mathbf{u}(\mathbf{x}, t)$  is the horizontal velocity field,  $\nabla$  is the 2D gradient operator and  $\mathbf{k}$  is the vertical unit vector. Many geophysical processes occur on approximately horizontal scales, where the vertical, gravity oriented, velocity component is several orders of magnitude smaller than the horizontal velocity component (Wayne, 2011). For example, in the case of dipole–dipole interactions, Dubosq and Viúdez (2007) investigated numerically non-axial frontal collisions of mesoscale baroclinic dipoles as well as 2D dipole collisions, and concluded that the 3D inelastic interaction processes were qualitatively similar to the 2D interactions, as long as, the vortices had a similar vertical extent. In this study, where we deal with elastic interactions, the two-dimensional processes are expected to be dominant. Our aim here is to understand the 2D dynamics of elastic interactions, as a first step to correctly understand the more complicated 3D elastic interactions of balanced, that is in absence of inertia–gravity waves, flows.

The basic fluid dynamic equations, leading to the material conservation of vertical vorticity, are briefly introduced in section 2. In the following section 3, the initial vorticity conditions are explained. The dipole model used is based on the two-dimensional Lamb–Chaplygin (L-C) dipole (Chaplygin, 2007), which is an exact theoretical dipole model that translates rigid and straight with constant speed, while the target vortex has a radial vorticity distribution given by the Bessel function of 0-order  $J_0(r)$ . In the next step, section 4, we describe numerical results showing that the dipole may be scattered by vortices, changing drastically its direction without modifying its vorticity distribution significantly, making possible elastic interactions. Finally concluding remarks are given in section 5.

## 2 Basic Equations

In 2D isochoric flows the stream function  $\psi(\mathbf{x}, t)$  provides the horizontal velocity  $\mathbf{u}(\mathbf{x}, t)$

$$\mathbf{u} \equiv -\nabla \times (\psi \mathbf{k}), \quad (1)$$

and vertical vorticity  $\zeta(\mathbf{x}, t)$

$$\zeta \equiv \mathbf{k} \cdot \nabla \times \mathbf{u} = \nabla^2 \psi, \quad (2)$$

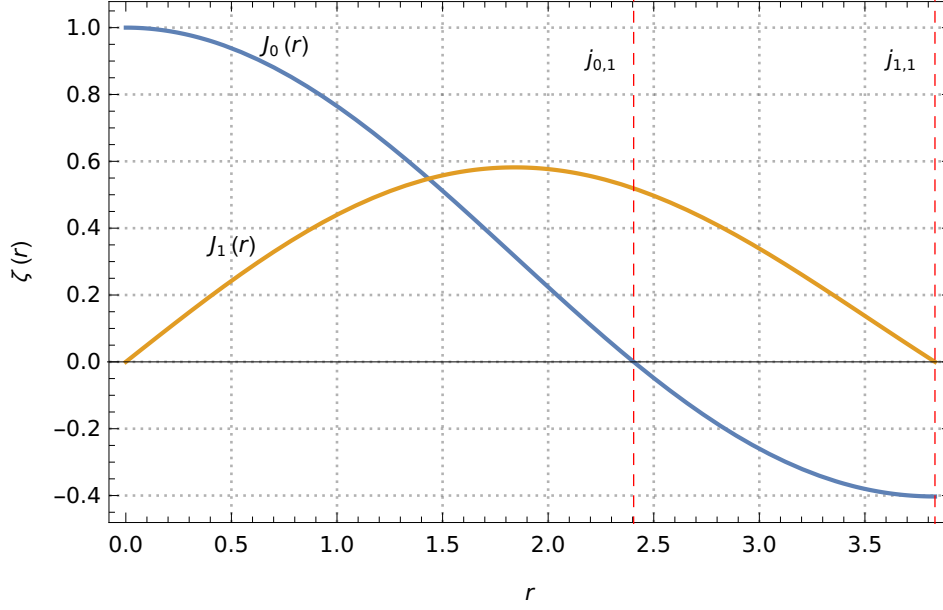


**Figure 1.** Bessel functions  $J_0(r)$  (blue) and  $J_1(r)$  (yellow). The red line stands for the zeroes  $j_{0,1}$  and  $j_{1,1}$

111 where  $\mathbf{k}$  is the vertical unit vector and  $\nabla$  is the 2D gradient operator. The basic  
 112 dynamical equation is the material conservation of vorticity

$$113 \quad \frac{d\zeta}{dt} \equiv \frac{\partial \zeta}{\partial t} + \mathbf{u} \cdot \nabla \zeta = 0. \quad (3)$$

114 Equation (3) is numerically integrated (a brief description is given in Appendix A) to  
 115 evolve in time the vorticity field from the initial vorticity conditions described in the  
 116 next section.

### 117 **3 Initial Conditions: Lamb-Chaplygin Dipole and Axisymmetrical Vor-** 118 **tex**

119 We use the Lamb-Chaplygin dipole model whose vorticity distribution  $\zeta_d(r, \theta)$  in  
 120 polar coordinates  $(r, \theta)$  is a piecewise function given by

$$121 \quad \zeta_d(r, \theta) \equiv \begin{cases} C_d J_1(k_1 r) \sin \theta & 0 \leq k_1 r \leq j_{1,1} \\ 0 & j_{1,1} < k_1 r \end{cases}, \quad (4)$$

122 where  $C_d$  is a constant vorticity amplitude,  $J_m(r)$  is the Bessel function of order  $m$ ,  
 123  $j_{m,n}$  is the  $n$ th zero of  $J_m(r)$  (Figure 1) and  $k_1$  is the dipole's wavenumber. This  
 124 dipole moves, in absence of background velocity, straight along the  $x$ -axis with a  
 125 constant speed equal to  $u_0 = -C_d J_0(j_{1,1}) / (2k_1)$ . The interior and exterior velocity  
 126 fields  $\mathbf{u}_d(r, \theta)$ , in polar coordinates, are given by

$$127 \quad \frac{\mathbf{u}_d(r, \theta)}{C_d/k_1} \equiv \begin{cases} \frac{J_1(k_1 r)}{k_1 r} \cos \theta \mathbf{e}_r - \frac{1}{2} (J_0(k_1 r) - J_2(k_1 r)) \sin \theta \mathbf{e}_\theta & 0 \leq k_1 r \leq j_{1,1} \\ \frac{J_0(j_{1,1})}{2k_1^2 r^2} [(k_1^2 r^2 - j_{1,1}^2) \cos \theta \mathbf{e}_r - (k_1^2 r^2 + j_{1,1}^2) \sin \theta \mathbf{e}_\theta] & j_{1,1} < k_1 r \end{cases}, \quad (5)$$

128 where  $\mathbf{e}_r$  and  $\mathbf{e}_\theta$  are the radial and azimuthal unit basis vectors.

129 In order to provide flow solutions with vanishing velocity at infinity we must  
 130 add to the steady piecewise flow (5) a background flow  $\mathbf{u}_0(\mathbf{x})$ , applied to the complete

131 spatial domain, such that the exterior velocity  $\mathbf{u}_d(r, \theta) \rightarrow \mathbf{0}$  as  $kr \rightarrow \infty$ . The new  
 132 solutions are time dependent and in Cartesian coordinates  $(x, y)$  are expressed as  
 133 follows

$$134 \quad \bar{\mathbf{u}}_d(x, y, t) \equiv \mathbf{u}_d(r(x - u_0 t, y), \theta(x - u_0 t, y)) + u_0 \mathbf{e}_r, \quad (6)$$

135 where  $\mathbf{u}_d(r, \theta)$  is the velocity field (5) in the steady state,  $r(x, y) = \sqrt{x^2 + y^2}$  and  
 136  $\theta(x, y) = \arctan(y/x)$ .

137 The vorticity distribution  $\zeta_v(r, \theta)$  of the axisymmetrical vortex is given by the  
 138 Bessel function of order 0 (Figure 1), truncated at a radius  $r = j_{0,1}/k_2$ , that is

$$139 \quad \zeta_v(r, \theta) \equiv \begin{cases} C_v J_0(k_2 r) & 0 \leq k_2 r \leq j_{0,1} \\ 0 & j_{0,1} < k_2 r \end{cases}, \quad (7)$$

140 where  $C_v$  is a constant vorticity amplitude and  $k_2$  is the vortex's wavenumber. The  
 141 vortex velocity  $\mathbf{u}_v(r) = v(r)\mathbf{e}_\theta$  is azimuthal and is given by

$$142 \quad \frac{v(r)}{C_v/k_2} \equiv \begin{cases} J_1(k_2 r) & 0 \leq k_2 r \leq j_{0,1} \\ \frac{J_1(j_{0,1})j_{0,1}}{k_2 r} & j_{0,1} < k_2 r \end{cases}. \quad (8)$$

143 When both, vortex and dipole, are present they interact due to their exterior  
 144 potential flows. This interaction depends on the vortices amplitude ( $C_d, C_v$ ) and vortices  
 145 extension given by the wavenumbers ( $k_1, k_2$ ). We are interested in interactions  
 146 between vortices with equal size and amplitude and therefore we set the positive cir-  
 147 culation of the dipole ( $\Gamma_d^+$ ) equal to the circulation of the vortex ( $\Gamma_v^+$ ), and the area of  
 148 the vortex ( $A_v$ ) equal to the area of the positive vorticity of the dipole ( $A_d^+$ ), that is

$$149 \quad \Gamma_d^+ = \Gamma_v^+, \quad A_d^+ = A_v. \quad (9)$$

150 The radius of the vortex is  $R_v = j_{0,1}/k_2$ , which implies  $A_v = \pi(j_{0,1}/k_2)^2$ . Since the  
 151 radius of the dipole is  $R_d = j_{1,1}/k_1$ , the area is  $A_d^+ = \pi(j_{1,1}/k_1)^2/2$  and applying (9),  
 152 we obtain the wavenumber ratio

$$153 \quad \frac{k_1}{k_2} = \frac{1}{\sqrt{2}} \frac{j_{1,1}}{j_{0,1}} \simeq 1.127. \quad (10)$$

154 The amplitudes ratio  $C_v/C_d$  is obtained from the circulation of the vortex and  
 155 the positive part of the dipole. The positive circulation of the dipole is

$$156 \quad \frac{\Gamma_d^+}{C_d} = \int_0^\pi \sin \theta d\theta \int_0^{j_{1,1}/k_1} J_1(k_1 r) r dr = -\frac{\pi}{k_1^2} j_{1,1} H_1(j_{1,1}) J_0(j_{1,1}), \quad (11)$$

157 where  $H_1(x)$  is the Struve function of order 1. The circulation of the vortex is

$$158 \quad \frac{\Gamma_v^+}{C_v} = \int_0^{2\pi} d\theta \int_0^{j_{0,1}/k_2} J_0(k_2 r) r dr = \frac{2\pi}{k_2^2} j_{0,1} J_1(j_{0,1}), \quad (12)$$

159 and therefore applying (9) we obtain the vorticity amplitudes ratio

$$160 \quad \frac{C_d}{C_v} = -\frac{j_{1,1} J_1(j_{0,1})}{H_1(j_{1,1}) J_0(j_{1,1}) j_{0,1}} \simeq 1.889. \quad (13)$$

161 The initial vorticity distribution is represented in figure 2. The dipole's poles  
 162 are close together and have the same vorticity contours as the axisymmetrical vortex.  
 163 The initial interaction between both vortices, as inferred from the stream function is  
 164 negligible. This initial vorticity distribution is integrated in time following the steps  
 165 explained in Appendix A. In the next section, we describe the numerical results of the  
 166 elastic interaction between both vortices.

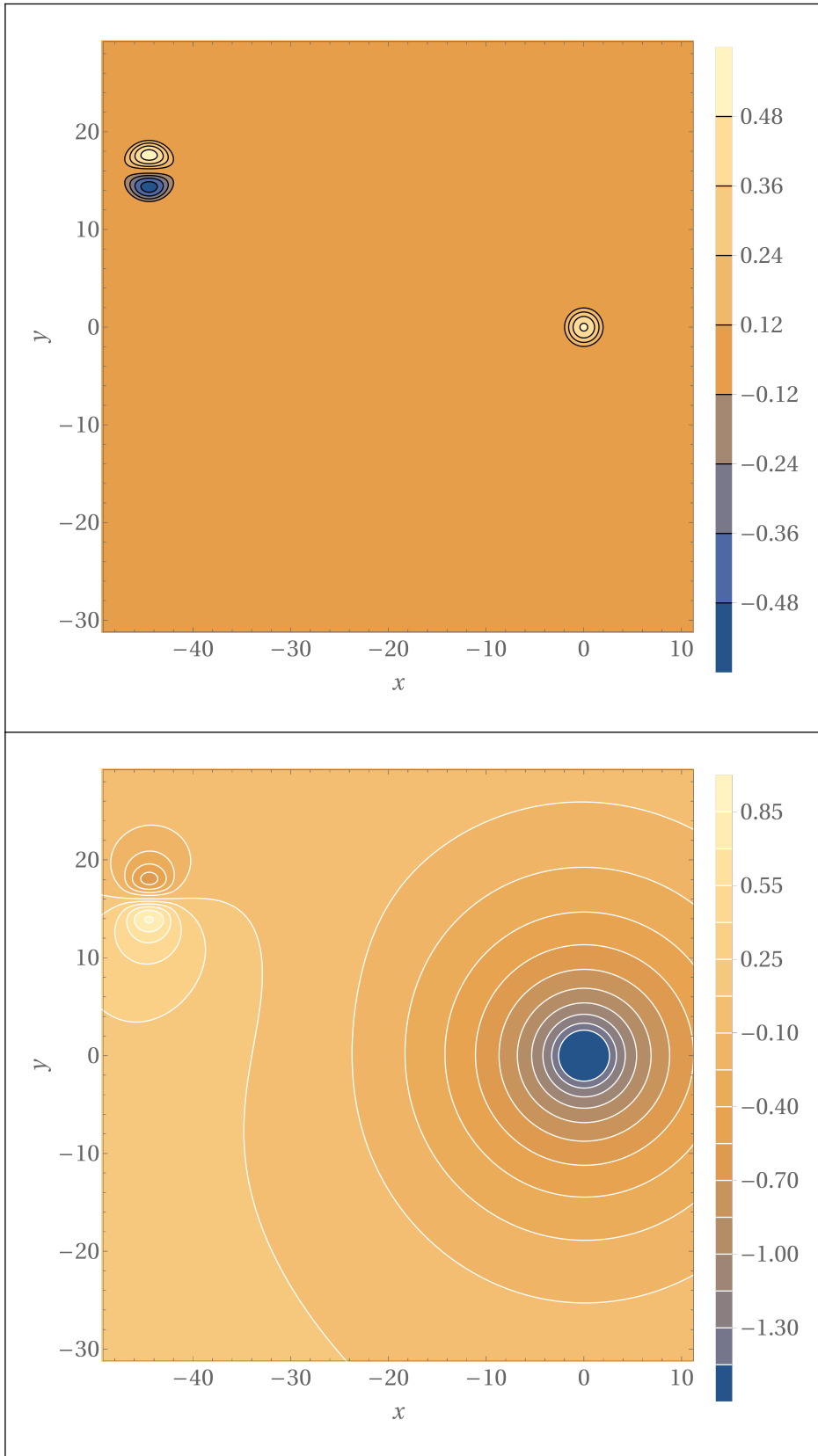


**Figure 2.** Vorticity (top) and stream function (bottom) distributions at  $t = 0$ .

## 4 Numerical Results

This section analyses numerically the interaction between the L-C dipole and the axisymmetrical vortex, with the initial vorticity distributions explained in the previous section. The time-dependent center positions of the positive and negative vorticity parts of the L-C dipole ( $\mathbf{r}_d^+(t)$  and  $\mathbf{r}_d^-(t)$ , respectively) are defined as

$$\mathbf{r}_d^\pm(t) \equiv \frac{\int_{A_d^\pm} (x, y) \tilde{\zeta}(x, y, t) dx dy}{\int_{A_d^\pm} \tilde{\zeta}(x, y, t) dx dy}, \quad (14)$$

where  $A_d^\pm$  are the time-dependent regions of points  $(x, y, t)$  where  $\pm\tilde{\zeta}(x, y, t) > 0$ . The time-dependent center of the whole dipole  $\mathbf{r}_d$  is given by

$$\mathbf{r}_d(t) \equiv \frac{\mathbf{r}_d^+(t) + \mathbf{r}_d^-(t)}{2}. \quad (15)$$

The time-dependent center position of the axisymmetrical vortex  $\mathbf{r}_v(t)$  is defined in an analogous way to (14).

Initially the dipole moves with an almost straight trajectory approaching the axisymmetrical vortex (Figure 3). As the dipole gets closer to the target vortex, the dipole-vortex interaction increases due to the potential background-flows of both vortices. As a result of this interaction the dipole is attracted by the vortex and its trajectory acquires negative curvature (Figure 3). On the other hand, the axisymmetrical vortex is also attracted by the dipole's potential-flow, and is slightly accelerated towards the approaching dipole (Figure 3). The closer the vortices get, the dipole's speed of displacement decreases (Figure 4) due to the fact that the dipole poles open up relative to the dipole's axis (Figures 3 and 5). At the time of highest pole separation ( $t \simeq 123$ ) the dipole's speed of displacement reaches a minimum (Figure 4) and the two centers of the vortices, as well as the centers of the poles, are completely alligned (Figure 3).

In this case, due to the large north-south initial distance between the dipole and the axisymmetrical vortex, there is no vorticity exchange between the vortices. After the time of largest interaction ( $t \simeq 123$ , Figure 5), the dipole's poles close and the dipole acquires a rigid vorticity distribution which is similar to its initial one but rotated positively (Figure 3).

The mechanism of the dipole's trajectory change, due to the interaction between the potential flows, involves a very small exchange of vorticity between the positive and negative poles and also in a small vorticity leakage, of both positive and negative vorticity, to the background field. While a L-C dipole consisting only on the first vorticity mode  $J_1(k_1 r)$ , dipolar antisymmetrical mode, moves along a straight trajectory, the presence of the zero mode  $J_0(k_2 r)$ , or rotational symmetrical mode, provides a constant curvature to the dipole's trajectory. In this numerical experiment the dipole, consisting initially of only the first vorticity mode  $J_1(k_1 r)$ , develops a small rotational mode via vorticity exchange between the poles while approaching the axisymmetrical vortex. The direction of this vorticity exchange is reversed as the dipoles leaves the vortex, in such a way that the mode-0 vanishes and the poles recover their antisymmetrical vorticity distribution. On the other side, the axisymmetrical vortex decelerates towards a new position very close to its initial location (Figure 3). The whole interaction process is shown in the video referenced in Figure 6.

The dipole's speed of displacement after the interaction is very close to its original value (Figure 4). This interaction, practically involving no net vorticity change between initial and final dipole vorticity distributions, may be classified as an elastic scattering of a vortex dipole by an axisymmetrical vortex. Nevertheless, it is important to underline that changes in the initial vorticity distribution of the axisymmetrical

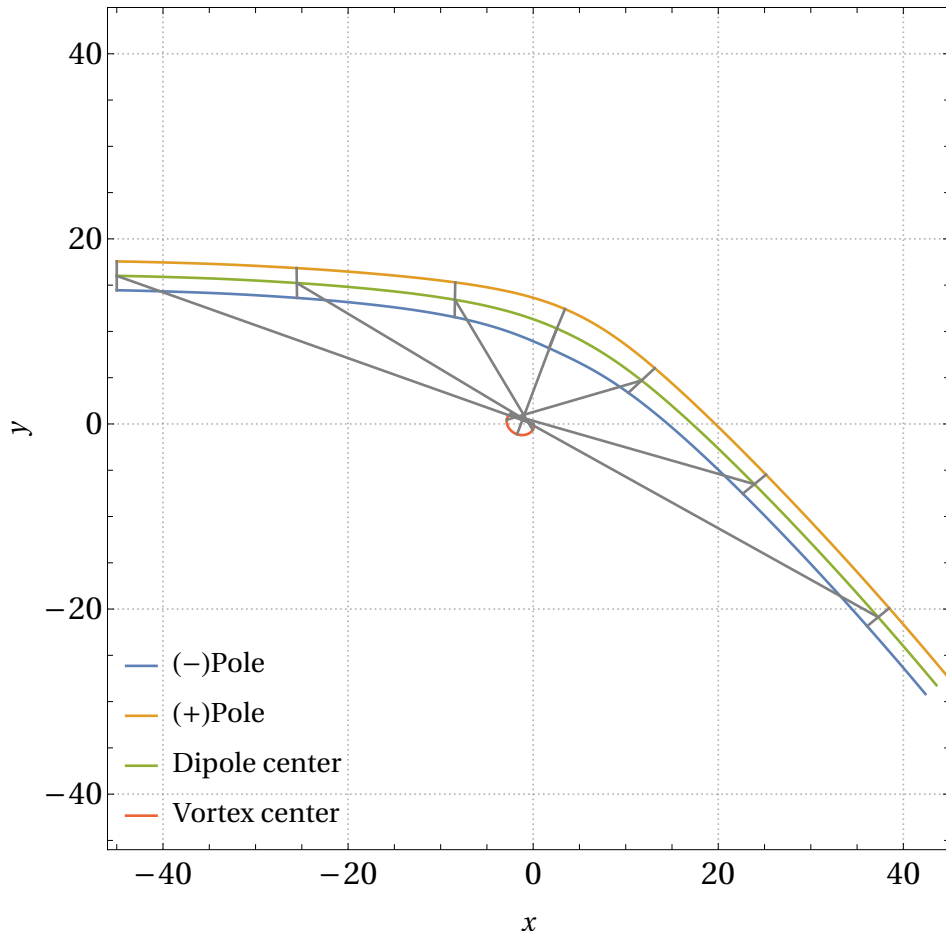


**Figure 3.** Trajectories of the center of the dipole poles  $\mathbf{r}^-(t)$  (blue),  $\mathbf{r}^+(t)$  (orange), the center of the whole dipole  $\mathbf{r}_d(t)$  (green), and the center of the axisymmetrical vortex  $\mathbf{r}_v(t)$  (red). The gray lines connect the + and - pole centers and the center of the dipole with the center of the vortex at seven different times.

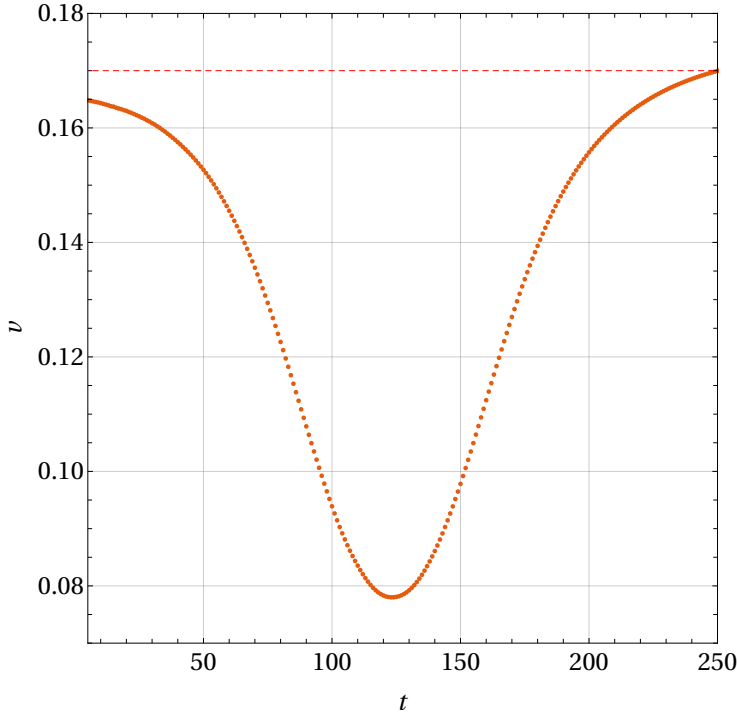


**Figure 4.** Dipole’s speed of displacement  $v_d(t) \equiv |\mathbf{dr}_d(t)/dt|$ . The dashed red line marks the speed of displacement of the last point.

214 vortex this interaction may lose its elastic behaviour. For example, if the vortex  
 215 vorticity boundary  $R_v$  is extended to the first zero  $j_{1,1}/k_2$ , in such a way that the vortex  
 216 vorticity distribution is  $\zeta(r)/C_v = J_0(k_2 r) - J_0(j_{1,1})$ , so that there is no vorticity  
 217 jump at the vortex boundary  $\zeta(j_{1,1}/k_2) = 0$ , the interaction is fully inelastic. In this  
 218 case it occurs an exchange of the negative vorticity pole between the dipole and the  
 219 axisymmetrical vortex. This example is described in more detail in Appendix B.

220 We have also analyzed interactions similar to the one described before but chang-  
 221 ing the initial positions of the dipole along the  $y$ -axis (video referenced in Figure 7).  
 222 In this video, the dipole with green vorticity contours at the top simulates the elastic  
 223 interaction described above. The dipole with black vorticity contours is located  
 224 half the way of the green dipole. This interaction is really similar to the interaction  
 225 described in Appendix B where the dipole is scattered by the axisymmetrical vortex  
 226 and the dipole’s poles separate. When the negative pole is close to the positive ax-  
 227 isymmetrical vortex, these two vortices join together, giving rise to partner exchange  
 228 and formation of a new dipole (video in Figure 7). The positive vorticity pole is left  
 229 behind and evolves towards an axisymmetrical vortex close to the initial position of  
 230 the initial axisymmetrical vortex.

231 The next dipole, with yellow vorticity contours, is located at the same  $y$ -coordinate  
 232 as the axisymmetrical vortex ( $y = 0$ ). In this case the vortices collide and merging  
 233 occurs (video in Figure 7). The next two dipoles, with white and red vorticity con-  
 234 tours, are situated at the same distance as the vortices black and green, respectively,  
 235 but with reversed sign, so that the positive pole of the dipole is the closest pole to  
 236 the axisymmetrical vortex. In these cases a positive-positive pole interaction occurs.  
 237 The white dipole, closer to the axisymmetrical vortex, suffers straining out vorticity  
 238 processes, while the red dipole, far from the axisymmetrical vortex, experiences also

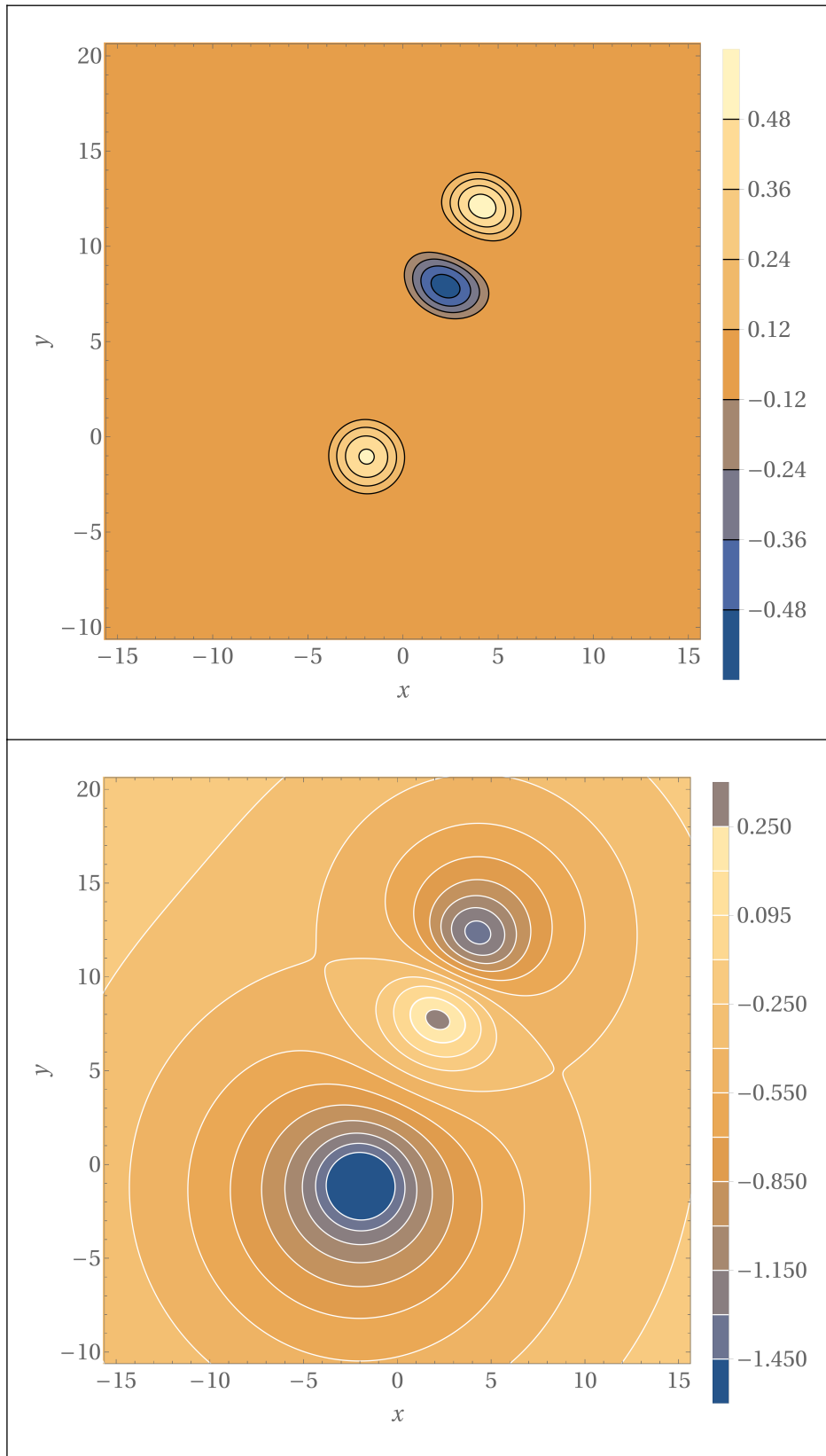


**Figure 5.** Vorticity (top) and stream function (bottom) distributions at the time of maximum poles separation ( $t = 123$ ).

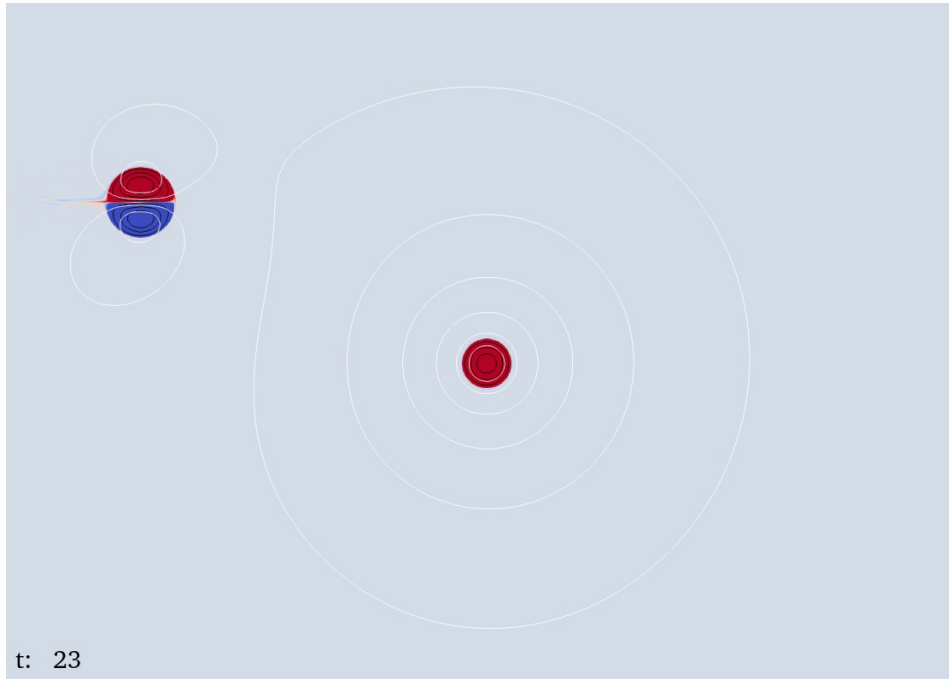


**Figure 6.** Video of the inelastic interaction between the dipole and the axisymmetrical vortex. The colour scale is saturated for a better visualization of the small vorticity changes. Blue and red colors mean negative and positive vorticity, respectively. Vorticity contour lines (black) and stream function contour lines (white) are included.

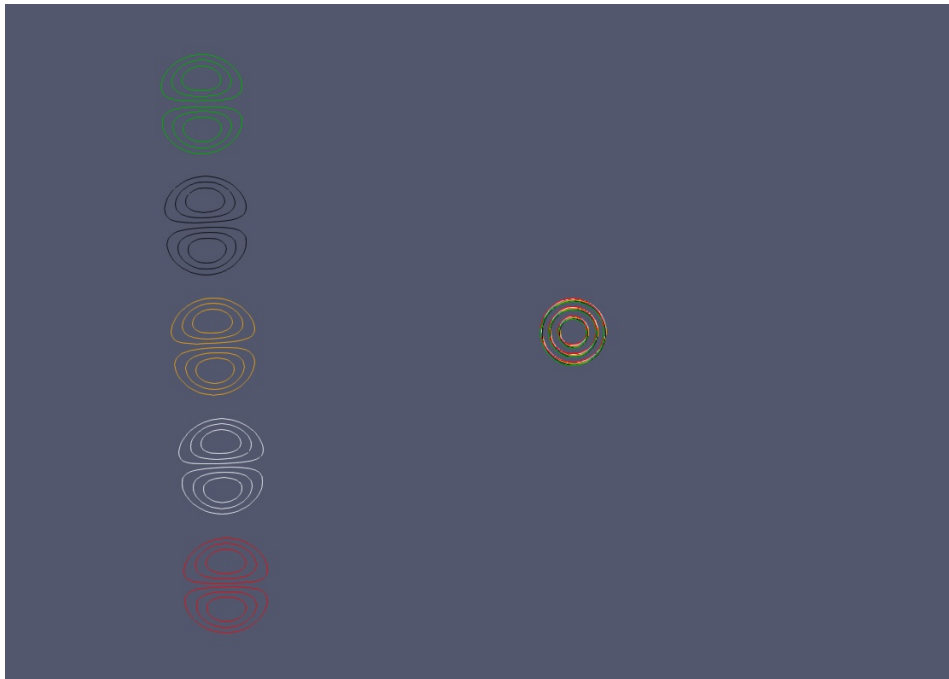


**Figure 7.** Superposition of five different simulations, represented with different vorticity contour line colors, of the interaction between the dipole and the axisymmetrical vortex. Each dipole starts at a different  $y$ -axis position. The axisymmetrical vortex is always placed at the position  $(0, 0)$ .

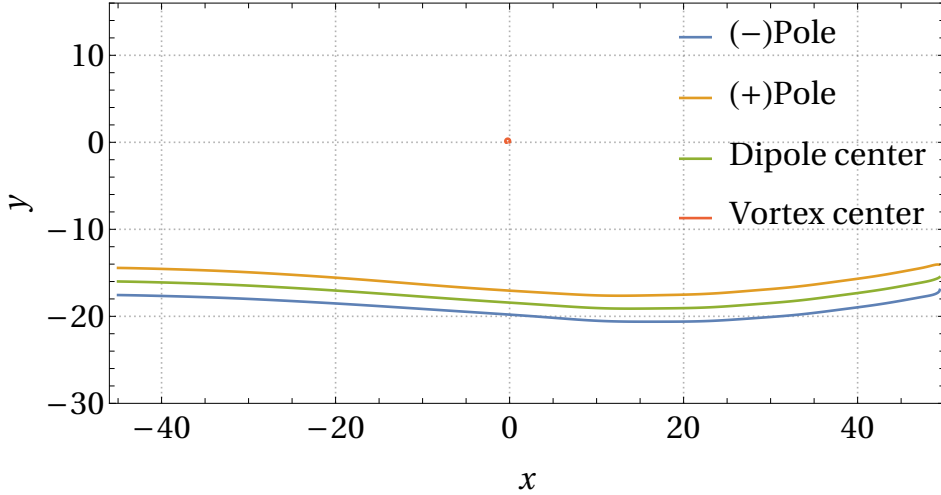


**Figure 8.** Trajectories of the center of the dipole poles  $\mathbf{r}^-(t)$  (blue),  $\mathbf{r}^+(t)$  (orange), the center of the whole dipole  $\mathbf{r}_d(t)$  (green), and the center of the axisymmetrical vortex  $\mathbf{r}_v(t)$  (red).

239 an elastic interaction but weaker than the one experienced by the green dipole (video  
 240 in Figure 7). In this case the red dipole is slightly repelled, instead of being attracted,  
 241 by the axisymmetrical vortex, in such a way that the dipole changes only slightly its  
 242 direction during the interaction time, to afterwards return to a straight trajectory with  
 243 the same initial direction. The axisymmetrical vortex behaves similar to the dipole,  
 244 it is repelled by the potential flow of the dipole and describes an almost semi-circular  
 245 trajectory with a small radius  $\delta r \simeq 0.6$  (too small to be appreciated in Figure 8) and  
 246 returns, after the interaction time, to a new location very close to the initial one.

247 Though this is a simple two-dimensional flow study, the application to three-  
 248 dimensional balanced geophysical flows is straightforward under the quasi-geostrophic  
 249 (QG) approximation. This is so because the two-dimensional initial vorticity con-  
 250 ditions chosen are naturally applicable to the theory of baroclinic QG flows where  
 251 the role played by the geopotential  $\phi(\mathbf{x}, t)$ , horizontal geostrophic velocity  $\mathbf{u}_h^g(\mathbf{x}, t) \equiv$   
 252  $\mathbf{k} \times \nabla \phi(\mathbf{x}, t)$  and the materially conserved QG potential vorticity anomaly  $\varpi^q(\mathbf{x}, t) =$   
 253  $\nabla^2 \phi(\mathbf{x}, t)$ , in the three-dimensional QG space, is equivalent to the role played by the  
 254 stream function  $\psi(\mathbf{x}_h, t)$ , horizontal velocity  $\mathbf{u}_h(\mathbf{x}_h, t) \equiv \mathbf{k} \times \nabla \psi(\mathbf{x}_h, t)$  and the ma-  
 255 terially conserved vertical vorticity  $\zeta(\mathbf{x}_h, t) = \nabla^2 \psi(\mathbf{x}_h, t)$  in the 2D isochoric flows  
 256 considered here. In three-dimensional QG flows, instead of the Bessel functions of the  
 257 first kind  $J_n(r)$ , which are the eigenfunctions of the radial part of the Laplacian oper-  
 258 ator in polar coordinates  $(r, \theta)$ , the relevant modes are the spherical Bessel functions  
 259 of the first kind  $j_l(\rho)$  and the spherical harmonics  $Y_l^m(\vartheta, \varphi)$ , of degree  $l$  and order  $m$ ,  
 260 which are the eigenfunctions of the radial part  $(\rho)$  and the angular part  $(\vartheta, \varphi)$ , respec-  
 261 tively, of the Laplacian operator in spherical coordinates  $(\rho, \vartheta, \varphi)$ . This approach has  
 262 been used recently to investigate three-dimensional baroclinic dipoles (Viúdez, 2019).

## 263 5 Concluding Remarks

264 In this work we have proved, using numerical simulations, that fully elastic inter-  
 265 actions between a vortex dipole and an axisymmetrical vortex are possible in two-  
 266 dimensional inviscid incompressible flows. In the particular example described in detail  
 267 here, a Lamb-Chaplygin dipole is elastically scattered by an axisymmetrical vortex.  
 268 When the initially straight moving L-C dipole approaches the target vortex they in-  
 269 teract due to their corresponding potential flows, in such a way that the dipole's

270 trajectory acquires curvature and the dipole’s vorticity poles open up. Once the L-C  
 271 dipole moves away from the target vortex, the dipole’s poles close and the dipole con-  
 272 tinues with a straight trajectory but with a direction different from the initial one. No  
 273 vorticity exchange between the dipole and the axisymmetrical vortex occurs, though  
 274 there is a small vorticity exchange between the poles and a small vorticity leakage to  
 275 the background field.

276 This description of an elastic interaction contributes to several previous stud-  
 277 ies involving dipoles interactions, including interactions of dipoles with solid bound-  
 278 aries (de Ruijter et al., 2004; Kloosterziel et al., 1993; Voropayev & Afanasyev, 1992;  
 279 Zavala Sansón & Gonzalez, 2021), interactions of dipoles with inertia-gravity waves  
 280 (Claret & Viúdez, 2010; Huang et al., 2017), and dipole-dipole interactions (Dubosq  
 281 & Viúdez, 2007; McWilliams & Zabusky, 1982; Velasco Fuentes & Heijst, van, 1995;  
 282 Voropayev & Afanasyev, 1992). In the cases of dipole-dipole and dipole-vortex interac-  
 283 tions both elastic and inelastic processes are possible depending on the initial vorticity  
 284 distribution, which includes the location, orientation and vorticity distributions of the  
 285 vortices. In the main example shown in this work, due to the particular initial con-  
 286 ditions chosen, inelastic interactions do not occur and the dipole-vortex interaction is  
 287 practically elastic. We have also seen that a change in the vorticity distribution of  
 288 the axisymmetrical vortex may lead to inelastic interactions involving vortex partner  
 289 exchange.

290 The results shown in this work are applicable to three-dimensional baroclinic  
 291 geophysical flows under the quasi-geostrophic (QG) approximation, as the initial vor-  
 292 ticity distributions are based on the eigenfunctions of the two-dimensional Laplacian  
 293 operator in circular geometry (the Bessel-azimuthal vorticity modes). Our future work  
 294 is to investigate the stability of isolated geophysical vortices, including also vortex in-  
 295 teractions, extending the approach of Viúdez (2021) in 2D to three-dimensional QG  
 296 flows.

## 297 Appendix A Scheme of the Numerical Algorithm

298 Given an initial vorticity field  $\zeta(x, y, t_0)$  the vorticity time integration is done in  
 299 four steps.

- 300 1. The stream function  $\psi(x, y, t_0)$  is obtained by solving (2) espectrally.
- 301 2. The velocity  $\mathbf{u}(x, y, t_0)$  is computed from  $\psi(x, y, t_0)$  using (1).
- 302 3. The vorticity advection  $-\mathbf{u} \cdot \nabla \zeta$  is computed in the physical space.
- 303 4. The vorticity at the next time-step  $\zeta(x, y, t_0 + \delta t)$  is obtained from (3) as

$$304 \quad \zeta(x, y, t_0 + \delta t) = -\delta t \mathbf{u} \cdot \nabla \zeta + \zeta(x, y, t_0).$$

305 After the step 4 the loop returns to step 1 for the next time integration ( $t_0 + \delta t$ ).  
 306 The numerical simulations were carried out using a 2D pseudospectral code where the  
 307 vorticity field  $\zeta(x, y, t)$  is numerically integrated, following the steps described above,  
 308 in a doubly periodic domain using an explicit leap-frog time-stepping method, together  
 309 with a weak Robert-Asselin time filter to avoid the decoupling of even and odd time  
 310 levels. The numerical domain was discretized in  $2048^2$  grid points.

## 311 Appendix B Dependence with the Radial Vorticity Profile of the Ax- 312 isymmetrical Vortex

313 In this case the axisymmetrical vortex boundary  $R_v$  is extended to the first zero  
 314  $R_v = j_{1,1}/k_2$ , instead of  $j_{0,1}/k_2$  (Figure 1), and its vorticity distribution is given by  
 315  $\zeta(r)/C_v = J_0(k_2 r) - J_0(j_{1,1})$  so that  $\zeta(j_{1,1}/k_2) = 0$  with no vorticity jump at the vortex  
 316 boundary. The other initial conditions described in section 3 remain unchanged. In

317 the general case where the vortex boundary is taken at  $k_2r = j_{m,n}$  the external flow  
318  $\mathbf{u}_0(r)$ , is given by

$$319 \quad \frac{\mathbf{u}_0(r)}{C_v/k_2} = \left[ \frac{J_0(j_{m,n})j_{m,n}^2}{2} - J_1(j_{m,n})\frac{j_{m,n}}{k_2r} \right] \mathbf{e}_\theta.$$

320 If the vortex boundary is taken at  $k_2r = j_{1,1}$  the external flow decays as  $C_v(J_0(j_{1,1})j_{1,1}^2/(2k_2^2r)) \simeq$   
321  $-2.9/(k_2^2r)$ , while if the vortex boundary is taken at  $k_2r = j_{0,1}$ , as in section 3,  
322 the external flow decays as  $-C_v(J_1(j_{0,1})j_{0,1}/(k_2^2r)) \simeq -1.2/(k_2^2r)$ , the ratio been  
323  $J_0(j_{1,1})j_{1,1}^2/(2J_1(j_{0,1})j_{0,1}) \simeq 2.4$ , indicates that the external flow in this example de-  
324 cays faster than the exterior flow in section 3.

325 In this case, the dipole moves initially with a straight trajectory approaching the  
326 axisymmetrical vortex. Then, the vortices are attracted by their potential flows and  
327 the poles of the dipole separate. The difference with the case studied in section 3 is  
328 that, in this case, while the poles open up the axisymmetrical vortex is pushed away  
329 from the dipole, and the negative pole of the dipole separates from the positive pole  
330 and joins the axisymmetrical vortex, giving rise to a new dipole (Figure B1). The  
331 positive pole of the dipole is left behind and remains as an axisymmetrical vortex close  
332 to the position of the original one.

### 333 Acknowledgments

334 We acknowledge the Spanish Ministerio de Ciencia e Innovacin for the FPI Ph.D. grant  
335 (PRE2019-090309).

### 336 References

- 337 Afanasyev, Y. (2003). Spontaneous emission of gravity waves by interacting vortex  
338 dipoles in a stratified fluid: Laboratory experiments. *Geophysical & Astrophys-*  
339 *ical Fluid Dynamics*, *97*(2), 79-95. doi: 10.1080/0309192031000114349
- 340 Ahlnäs, K., Royer, T. C., & George, T. H. (1987). Multiple dipole eddies in the  
341 Alaska Coastal Current detected with Landsat thematic mapper data. *Journal*  
342 *of Geophysical Research: Oceans*, *92*(C12), 13041-13047. doi: [https://doi.org/](https://doi.org/10.1029/JC092iC12p13041)  
343 [10.1029/JC092iC12p13041](https://doi.org/10.1029/JC092iC12p13041)
- 344 Barton, E. D., Arístegui, J., Tett, P., & Navarro-Pérez, E. (2004). Variability in  
345 the Canary Islands area of filament-eddy exchanges. *Progress in Oceanography*,  
346 *62*(2), 71-94. (The Canary Islands Coastal Transition Zone - Upwelling, Eddies  
347 and Filaments) doi: <https://doi.org/10.1016/j.pocean.2004.07.003>
- 348 Besse, V., Leblond, H., Mihalache, D., & Malomed, B. (2014). Building patterns  
349 by traveling dipoles and vortices in two-dimensional periodic dissipative me-  
350 dia. *Optics Communications*, *332*, 279-291. doi: [https://doi.org/10.1016/](https://doi.org/10.1016/j.optcom.2014.07.029)  
351 [j.optcom.2014.07.029](https://doi.org/10.1016/j.optcom.2014.07.029)
- 352 Carton, X. (2001, 05). Hydrodynamical modeling of oceanic vortices. *Surveys in*  
353 *Geophysics*, *22*, 179-263. doi: 10.1023/A:1013779219578
- 354 Chaplygin, S. (2007, 04). One case of vortex motion in fluid. *Regul. Chaot. Dyn.*, *12*,  
355 219-232. doi: 10.1134/S1560354707020074
- 356 Claret, M., & Viúdez, A. (2010, 12). Vertical velocity in the interaction between  
357 inertia-gravity waves and submesoscale baroclinic vortical structures. *Journal*  
358 *of Geophysical Research (Oceans)*, *115*, C12060. doi: 10.1029/2009JC005921
- 359 Couder, Y., & Basdevant, C. (1986, 12). Experimental and numerical study of vor-  
360 tex couples in two-dimensional flows. *Journal of Fluid Mechanics*, *173*, 225-  
361 251. doi: 10.1017/S0022112086001155
- 362 de Ruijter, W. P., van Aken, H. M., Beier, E. J., Lutjeharms, J. R., Matano, R. P.,  
363 & Schouten, M. W. (2004). Eddies and dipoles around South Madagas-  
364 car: formation, pathways and large-scale impact. *Deep Sea Research Part I:*

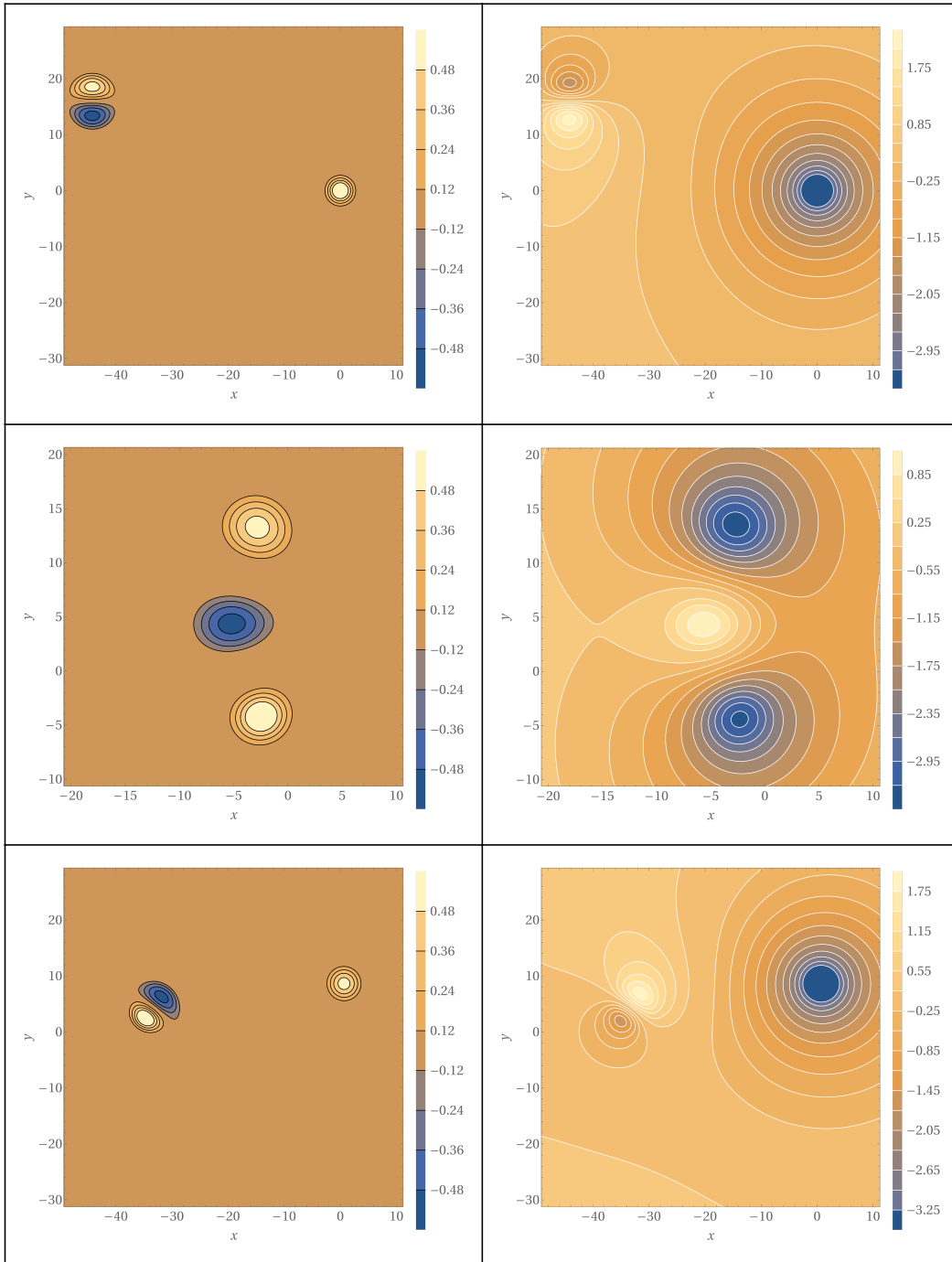


**Figure B1.** Time evolution of the vorticity (left) and stream function (right) of the inelastic interaction at times  $t=0$  (top),  $t=70$  (middle) and  $t=130$  (bottom).

- 365 *Oceanographic Research Papers*, 51(3), 383-400. doi: [https://doi.org/10.1016/](https://doi.org/10.1016/j.dsr.2003.10.011)  
366 [j.dsr.2003.10.011](https://doi.org/10.1016/j.dsr.2003.10.011)
- 367 Dritschel, D. G. (1995). A general theory for two-dimensional vortex interactions.  
368 *Journal of Fluid Mechanics*, 293, 269-303. doi: 10.1017/S0022112095001716
- 369 Dritschel, D. G., & Waugh, D. W. (1992). Quantification of the inelastic interaction  
370 of unequal vortices in two-dimensional vortex dynamics. *Physics of Fluids*, 4,  
371 1737-1744.
- 372 Dubosq, S., & Viúdez, A. (2007). Three-dimensional mesoscale dipole frontal col-  
373 lisions. *Journal of Physical Oceanography*, 37(9), 2331-2344. doi: 10.1175/  
374 JPO3105.1
- 375 Flór, J. B., & Van Heijst, G. J. F. (1994). An experimental study of dipolar vortex  
376 structures in a stratified fluid. *Journal of Fluid Mechanics*, 279, 1011-1033. doi:  
377 10.1017/S0022112094003836
- 378 Huang, X., Zhang, Z., Zhang, X., Qian, H., Zhao, W., & Tian, J. (2017). Impacts of  
379 a mesoscale eddy pair on internal solitary waves in the northern South China  
380 Sea revealed by mooring array observations. *Journal of Physical Oceanography*,  
381 47(7), 1539-1554.
- 382 Johannessen, J., Sandven, S., Lygre, K., Svendsen, E., & Johannessen, O. (1989,  
383 01). Three-dimensional structure of mesoscale eddies in the Norwegian Coastal  
384 Current. *Journal of Physical Oceanography - J PHYS OCEANOGR*, 19, 3-19.  
385 doi: 10.1175/1520-0485(1989)019<0003:TDSOME>2.0.CO;2
- 386 Kloosterziel, R. C., Carnevale, G. F., & Phillippe, D. (1993, 10). Propagation of  
387 barotropic dipoles over topography in a rotating tank. *Dynamics of Atmo-*  
388 *spheres and Oceans*, 19(1), 65-100. doi: 10.1016/0377-0265(93)90032-3
- 389 Li, Z., Wang, X., Hu, J., Andutta, F. P., & Liu, Z. (2020). A study on an  
390 anticyclonic-cyclonic eddy pair off Fraser Island, Australia. *Frontiers in Ma-*  
391 *rine Science*, 7, 1061. doi: 10.3389/fmars.2020.594358
- 392 McWilliams, J. C., & Zabusky, N. J. (1982, 01). Interactions of isolated vortices  
393 I: Modons colliding with modons. *Geophysical and Astrophysical Fluid Dynam-*  
394 *ics*, 19(3), 207-227. doi: 10.1080/03091928208208956
- 395 Rasmussen, J., Hesthaven, J., Lynov, J., Nielsen, A., & Schmidt, M. (1996). Dipolar  
396 vortices in two-dimensional flows. *Mathematics and Computers in Simulation*,  
397 40(3), 207-221. doi: [https://doi.org/10.1016/0378-4754\(95\)00033-X](https://doi.org/10.1016/0378-4754(95)00033-X)
- 398 Ridderinkhof, W., Le Bars, D., von der Heydt, A. S., & de Ruijter, W. P. M. (2013).  
399 Dipoles of the south east Madagascar Current. *Geophysical Research Letters*,  
400 40(3), 558-562. doi: <https://doi.org/10.1002/grl.50157>
- 401 Santiago-García, M. W., Parés-Sierra, A. F., & Trasviña, A. (2019, 12). Dipole-wind  
402 interactions under gap wind jet conditions in the Gulf of Tehuantepec, Mexico:  
403 A surface drifter and satellite database analysis. *PLOS ONE*, 14(12), 1-23.  
404 doi: 10.1371/journal.pone.0226366
- 405 Sheres, D., & Kenyon, K. E. (1989). A double vortex along the California coast.  
406 *Journal of Geophysical Research: Oceans*, 94(C4), 4989-4997. doi: [https://doi](https://doi.org/10.1029/JC094iC04p04989)  
407 [.org/10.1029/JC094iC04p04989](https://doi.org/10.1029/JC094iC04p04989)
- 408 Velasco Fuentes, O., & Heijst, van, G. (1995). Collision of dipolar vortices on a beta-  
409 plane. *Physics of Fluids*, 7(11), 2735-2750. doi: 10.1063/1.868652
- 410 Viúdez, A. (2019). Exact solutions of asymmetric baroclinic quasi-geostrophic  
411 dipoles with distributed potential vorticity. *Journal of Fluid Mechanics*, 868,  
412 R1. doi: 10.1017/jfm.2019.234
- 413 Viúdez, A. (2021). Robust and unstable axisymmetric vortices, including neutral  
414 vortices, of a new two-dimensional vortex family. *Physics of Fluids*, 33(5),  
415 054103. doi: 10.1063/5.0048128
- 416 Voropayev, S. I., & Afanasyev, I. D. (1992, 03). Two-dimensional vortex-dipole in-  
417 teractions in a stratified fluid. *Journal of Fluid Mechanics*, 236, 665-689. doi:  
418 10.1017/S0022112092001575
- 419 Voropayev, S. I., & Afanasyev, Y. D. (1994). *Vortex structures in a stratified fluid.*

- 420 Chapman and Hall.  
421 Wayne, C. E. (2011, 01). Vortices and two-dimensional fluid motion. *Notices of the*  
422 *American Mathematical Society*, 58, 10-19.  
423 Zavala Sansón, L., & Gonzalez, J. F. (2021). Travelling vortices over mountains and  
424 the long-term structure of the residual flow. *Journal of Fluid Mechanics*, 922,  
425 A33. doi: 10.1017/jfm.2021.567